

An Efficient Post-hoc Framework for Reducing Task Discrepancy of Text Encoders for Composed Image Retrieval

Jaeseok Byun^{1*} Seokhyeon Jeong^{1*} Wonjae Kim² Sanghyuk Chun^{2†} Taesup Moon^{1,3†}

¹Department of ECE, Seoul National University

²NAVER AI Lab

³ Department of ASRI/INMC/IPAI/AIIS, Seoul National University

Abstract

Composed Image Retrieval (CIR) aims to retrieve a target image based on a reference image and conditioning text, enabling controllable image searches. The mainstream Zero-Shot (ZS) CIR methods bypass the need for expensive training CIR triplets by projecting image embeddings into the text token embedding space, forming a composed query for retrieval. However, we highlight an inherent limitation in these projection-based CIR: a task discrepancy of text encoders between the original pre-training task of the encoders ($\text{text} \leftrightarrow \text{image}$) and the target CIR task ($\text{image} + \text{text} \leftrightarrow \text{image}$), which potentially negatively impacts CIR performance. To reduce such a discrepancy, a naive solution would be to train both image and text encoders with CIR triplets in a supervised manner. Instead, we introduce Reducing Task Discrepancy of Text Encoders (RTD), an efficient text-only post-hoc framework that complements projection-based CIR methods. We devise a novel target-anchored text contrastive learning designed to enhance the capability of the text encoder for CIR. We also propose two key enhancements: (1) a hard negative-based refined batch sampling strategy and (2) a refined concatenation scheme to further mitigate training-inference discrepancy. Integrating RTD into state-of-the-art projection-based methods achieves performance comparable to, or even surpassing, resource-intensive state-of-the-art synthetic CIR triplet-based approaches only with 23 minutes of additional training on 4 A100 GPUs—up to $100\times$ faster in training. Our code will be available upon acceptance.

1. Introduction

Composed Image Retrieval (CIR) aims at retrieving a target image that closely resembles a reference image while reflecting the changes described in a conditioning text. Using a

query composed of image and text allows users to conduct more precise and flexible searches by specifying the desired modifications to the image through text. Supervised CIR methods [2, 12, 21] have been introduced to fuse information from bi-modal query, using labeled data from the target domain in the form of triplets (I_r, T_c, I_t) , in which I_r is a reference image, T_c is a conditioning text, and I_t is a target image. However, unlike the typical web-crawled image-text datasets [38], acquiring sufficient triplets for training needs expensive manual human annotations. To overcome the dependency on small-scale and human-verified triplets of the target domain, several works utilize the power of recent generative models. For example, a line of studies [16, 22, 45, 48] uses text-to-image models like IP2P [5] or large-language models (LLM) [6, 43] to synthesize large-scale CIR triplets for training, in place of the target-domain CIR triplets. While these methods achieve strong performance, they are often impractical due to the high computational and memory requirements for utilizing generative models.

Another approach for removing the dependency on the CIR triplets, which often is referred to as projection-based ZS-CIR [4, 17, 26, 36, 41, 42], employs an integrable projection module on top of the pre-trained, frozen, and shared VL embedding space, such as CLIP [34]. Namely, a projection module ϕ , which maps a CLIP image embedding to the CLIP text token embedding space, can be trained by solely using images [4, 36] or texts [17]. During inference, as illustrated in Fig. 1, these methods first project the embedding of the query image to a text token embedding [extract_itex][\\$] using the function ϕ . This embedding is then combined with the conditioning text $[T_c]$ to create the prompt “a photo of [extract_itex][\\$] that [extract_itex>[T_c]”, which is used as a query for the text-to-image retrieval.

The core assumption of the projection-based CIR is that the pre-trained text encoder should be robust enough to combine information from both the projected text token embedding and the conditioning text. However, we argue that this can cause a significant *task discrepancy* for the pre-trained

*Equal contribution

†Corresponding authors

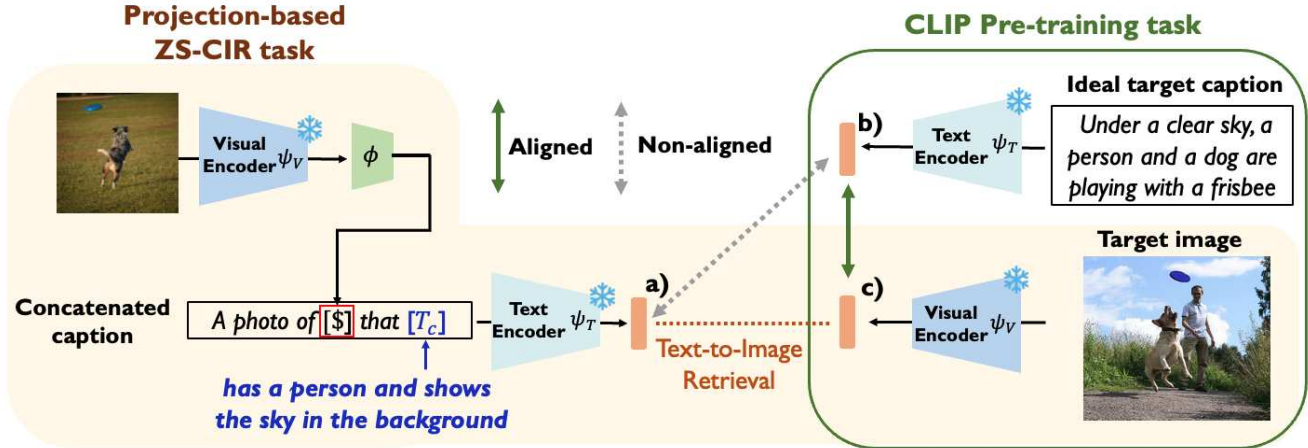


Figure 1. The task discrepancy of projection-based ZS-CIR methods between the pre-training task (image-text alignment) and the ZS-CIR task (image-text composition).

text encoder between the original image-text alignment pre-training task (of CLIP) and the CIR task. For example, in Fig. 1, consider an *ideal caption* that accurately describes the target image. Since the CLIP text and image encoders are learned through contrastive learning, we can expect that the target image embedding (Fig. 1c) will align well with the embedding (Fig. 1b) of the ideal caption. In contrast, in the projection-based CIR, the text encoder receives a concatenated caption that combines the projected token $[\$]$ and the conditioning text, not an ideal caption. However, as noted by Baldrati et al. [3], the text encoder is not typically trained to encode complex textual modifications—such as addition, negation, or replacement—to the reference image, which are common in conditioning texts. As a result, there is no guarantee that the textual embedding of the concatenated caption (Fig. 1a) closely aligns with the target image embedding (Fig. 1c), which will undermine the retrieval performance.

To that end, we devise a complementary post-processing approach for existing projection-based CIR methods that reduces the task discrepancy of the text encoder efficiently. Ideally, both image and text backbones would be updated using expensive CIR triplets (I_r, T_c, I_t) ; however, we achieve this using cheap *text* triplets and only update the text encoder. These text triplets (T_r, T_c, T_t) consist of a reference caption (T_r , e.g., “a dog catching a frisbee”), a conditioning text (T_c , e.g., “change dog to cat”), and a target caption (T_t , e.g., “a cat catching a frisbee”), respectively. Given that the reference captions T_r are readily available from conventional caption datasets, T_c and T_t can be automatically generated without any human labor [28, 46] or intensive resources [16, 22, 45, 48]. Using these triplets, we introduce a *target-anchored text contrastive learning*, in which the text encoder updates the embedding of the concatenated caption T_{r+c} of T_r and T_c (e.g., “a dog catching a frisbee”+ “change the dog to a cat”) to align closely with the fixed embedding of the target caption T_t from the frozen text encoder. We fur-

ther enhance this text-only training approach with two key components: a batch sampling strategy that ensures hard negatives in each mini-batch and a refined concatenation scheme for T_r and T_c designed to reduce the training-inference task discrepancy caused by our text-only training framework.

Our experimental results demonstrate that our proposed method, dubbed as **RTD** (Reducing Task Discrepancy of Text Encoders), consistently and considerably improves the performance in diverse evaluation datasets (CIRR [28], CIRCO [4], FashionIQ [46], COCO object composition [36], and GeneCIS [44]), when integrated with existing projection-based CIR methods (SEARLE [4], Pic2Word [36], LinCIR [17], Context-I2W [42], and FTI4CIR [26]). Consequently, compared to resource-intensive state-of-the-art synthetic CIR triplets-based method like MagicLens [48], RTD achieves comparable results, with less than a 1% gap in CIRR R@1 and 0.1% in FashionIQ R@10 when combined with FTI4CIR (ViT-L/14). When using larger or fine-tuned backbones (ViT-G/14 or FSC-CLIP [31]) with LinCIR, RTD achieves superior results than MagicLens in those metrics.

We note that RTD achieves the above results with significantly higher training efficiency in both data generation and training time. Specifically, our rule-based text triplet generation requires less than 10 minutes to construct 1M text triplets—570× faster than CIR triplet generation from Compodiff [16]. With 4 NVIDIA A100 GPUs, the additional training time for RTD is just 23 minutes for training the ViT-L/14 backbone, making it approximately 10 to 100× faster than synthetic CIR triplets-based methods. Even with a significantly larger backbone (ViT-G/14), training takes only 2.5 hours, remaining negligible in comparison. Moreover, we investigate the effectiveness of RTD across various text triplet generation strategies and different backbone sizes (ViT-B/32, ViT-L/14, ViT-G/14) and types (FSC-CLIP [31], CLIP [34]), showing its reproducibility and compatibility.

2. Related Work

Composed Image Retrieval. Unlike supervised CIR methods [2, 3, 12, 21], projection-based CIR methods [4, 13, 17, 26, 36, 41, 42] are built upon the frozen CLIP model, where a projection module ϕ is trained without CIR triplets. Each method employs a different training scheme for different training schemes for ϕ (See Sec. 4.1 for details). Several approaches avoid the need for any training by employing interpolation techniques [19], while others leverage powerful yet resource-intensive models such as LLMs and captioners [20, 47]. While our approach is built upon projection-based CIR methods, its training strategy is closely related to another category of CIR methods [16, 22, 45, 48] that use synthetically generated expensive CIR triplets. However, our method stands out by utilizing text triplets and updating only the text encoder, resulting in more efficient training while maintaining strong performance.

Task discrepancy between the CLIP pre-training task and CIR. Combiner [3] updates the text encoder to minimize the gap between the target caption feature and the sum of the reference image and conditioning text features. FashionERN [9] addresses reference image dominance by introducing a separate branch to amplify the impact of the conditioning text. However, both Combiner and FashionERN require expensive CIR triplets (I_r, T_c, I_t) for training, whereas our approach uses cheap, automatically generated text-only triplets (T_r, T_c, T_t) . As another example, Chen and Lai [7] synthesize a triplet of an original image, its caption, and the masked image, treating them as the target image, conditioning text, and reference image, respectively. This approach, however, still has a gap between conditioning text (*e.g.*, “change dog to cat”) and image caption (*e.g.*, “a dog catching a frisbee”); furthermore, it needs the full fine-tuning of the CLIP model, resulting in changing the visual embeddings in the retrieval database. In contrast, RTD directly uses the conditioning texts for training and does not change the target visual encoder, enabling the reuse of pre-extracted CLIP embeddings. Lastly, CIReVL [20] or LDRE [47] reduce task discrepancy by generating descriptive captions of the composed query using a large captioning model [24] and LLM [6]. While effective without any training, they rely on expensive inference steps and require carefully crafted prompts by skilled users. Whereas, RTD is fully automated, human-free, and more efficient during inference.

3. Main Method

3.1. Obtaining text triplets

To address the task discrepancy, we collect cheaply and automatically generated text triplets (T_r, T_c, T_t) , instead of directly using the expensive CIR triplets (I_r, T_c, I_t) . Given reference caption T_r from conventional caption datasets,

conditioning text T_c and target text T_t can be generated using two strategies: via large language models (LLMs) [5, 16, 22, 45] or, more efficiently, through rule-based templates [16]. We investigate both strategies and demonstrate that RTD consistently improves performance across them.

For the LLM-based strategy, we use the publicly available text triplets by CompoDiff [16], which are employed in our main experiments if not specified. These triplets are generated by taking a given caption T_r as an input of the fine-tuned LLM, whose output predicts the corresponding conditioning text T_c and the target caption T_t . Previous works, such as IP2P [5], CoVR [45], and CASE [22], have also explored generating text triplets using LLMs, differing in LLM model types, input data, and fine-tuning strategies. The original purpose of these text triplet generations is to construct CIR triplets (I_r, T_c, I_t) , but all these works also release the corresponding text triplets used for their CIR triplet construction. In addition to these publicly available text triplets, we also implement and evaluate an efficient in-context learning generation strategy using LLaMA3-8B [14] without additional fine-tuning. We conduct experiments with all the aforementioned text triplets in Tab. 6 and observe that RTD consistently delivers significant enhancements.

For cheap, rule-based strategy, we can extract a keyword (*e.g.*, “dog”) from T_r (“a dog catching a frisbee”) and replace it with a randomly chosen keyword (*e.g.*, “cat”) [16], forming T_c . The conditioning text is then generated automatically by using pre-defined templates (*e.g.*, “change [original keyword] to [altered keyword]”). Our experiments show that this simple rule-based variant performs similarly to the LLM-based one.

More detailed explanations and examples of each strategy are provided in App. A.2, and a comprehensive comparison of generation costs is provided in App. C.

3.2. Target-anchored text contrastive learning

Now, we explain our approach to update the text encoder for mitigating the task discrepancy solely with the generated text triplets (T_r, T_c, T_t) . We first assume that there exists a pre-trained projection module ϕ obtained by the projection-based ZS-CIR methods [4, 17, 36]. Recall that for a given reference image I_r and conditioning text T_c , the final composed feature is generated by passing the text prompt “a photo of $\phi(\psi_V(I_r))$ that T_c ” to the text encoder ψ_T , where ψ_V is the visual encoder and ϕ is the projection module (See Fig. 1). We aim to update the text encoder ψ_T to reduce the discrepancy between the pretext task and ZS-CIR task using the text triplets while maintaining ψ_V and ϕ frozen.

Target-anchored text contrastive loss. We apply contrastive learning using a paired caption (T_{r+c}, T_t) , where T_{r+c} denotes a concatenated caption of reference caption T_r and conditioning caption T_c . Namely, we let the representation of the concatenated caption closely approximate

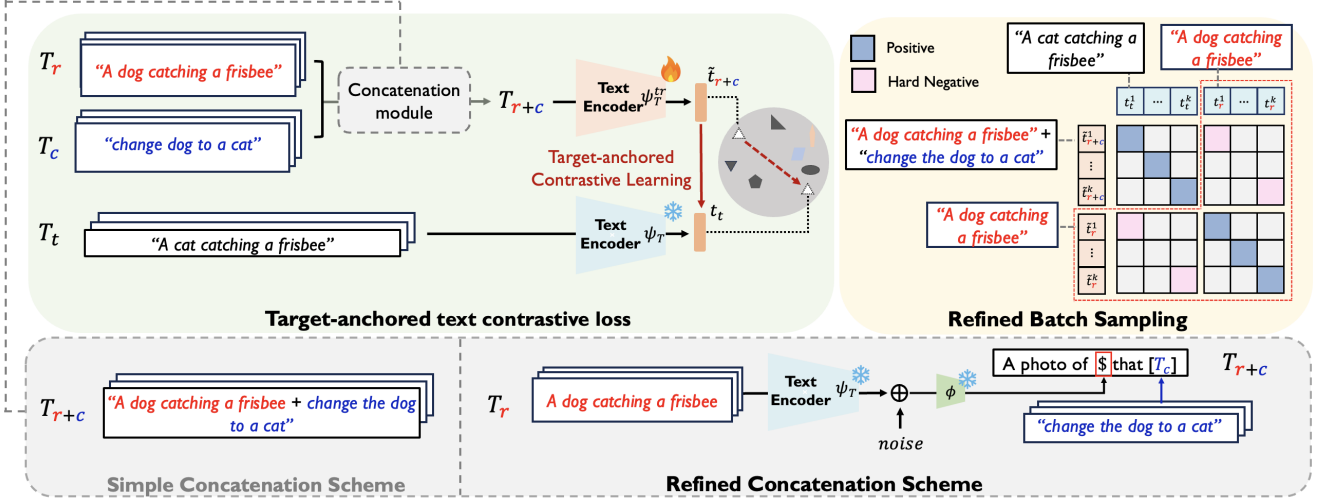


Figure 2. Overview of RTD.

that of the target caption. However, solely updating the text encoder while fixing the image encoder can break the alignment between image and text encoders. To prevent the issue, we extract the text embedding of T_t using the frozen text encoder ψ_T , while the concatenated caption T_{r+c} is extracted from the learnable text encoder ψ_T^{tr} , initialized from ψ_T . Here, we assume that as the target caption T_t is a standard caption, a text embedding $\psi_T(T_t)$, is well-aligned with the frozen image embedding space. Following the assumption, we fix the target textual embedding as an anchor point to maintain the pre-trained alignment while learning new relationships. As shown in Sec. 4.3, this anchoring is essential for fine-tuning the text encoder with our objective.

Now, we introduce our target-anchored text contrastive loss \mathcal{L}_{TCL} using two text encoders: a frozen pre-trained text encoder ψ_T and a learnable text encoder ψ_T^{tr} which is initialized with ψ_T . Textual latent embeddings \tilde{t}_{r+c} and t_t are extracted from ψ_T^{tr} and ψ_T , respectively. Namely, $\tilde{t}_{r+c} = \psi_T^{tr}(E_w^{tr}(T_{r+c}))$ and $t_t = \psi_T(E_w(T_t))$, where E_w is a word embedding layer. We aim to tune ψ_T^{tr} to minimize the distance between the concatenated textual embedding \tilde{t}_{r+c} and the target textual embedding t_t while maximizing the distance from other textual embeddings within the batch. We employ a symmetric InfoNCE loss [8, 11], as follows:

$$\begin{aligned}
 \mathcal{L}_{TCL} = & \frac{1}{B} \sum_{k=1}^B -\log \left(\frac{e^{(c(\tilde{t}_{r+c}^k, t_t^k)/\tau)}}{\sum_{j=1}^B e^{(c(\tilde{t}_{r+c}^k, t_t^j)/\tau)} + \sum_{j \neq k} e^{(c(t_t^k, \tilde{t}_{r+c}^j)/\tau)}} \right) \\
 & - \log \left(\frac{e^{(c(t_t^k, \tilde{t}_{r+c}^k)/\tau)}}{\sum_{j=1}^B e^{(c(t_t^k, \tilde{t}_{r+c}^j)/\tau)} + \sum_{j \neq k} e^{(c(\tilde{t}_{r+c}^k, \tilde{t}_{r+c}^j)/\tau)}} \right)
 \end{aligned} \quad (1)$$

in which $c(\cdot, \cdot)$ denotes the cosine similarity, B is the batch size, and τ is a temperature.

Refined batch sampling strategy for hard negatives. To further enhance the efficacy of updating the text encoder, we devise a simple yet effective batch sampling strategy that incorporates pairs of (T_{r+c}, T_t) and (T_r, T_r) within the same batch. For example, as presented in Fig. 2, a pair such as $(T_{r+c}: "A dog catching a frisbee + change dog to cat", T_t: "A cat catching a frisbee")$ is sampled along with its corresponding reference pair $(T_r: "A dog catching a frisbee", T_r: "A dog catching a frisbee")$ in the same batch. This setup ensures that the concatenated text T_{r+c} and its corresponding reference text T_r implicitly act as hard negatives for each other, as their semantics are much more similar (T_{r+c} is derived from T_r) than those of other randomly sampled texts in the batch. Explicitly distinguishing the embedding of T_{r+c} from that of T_r conceptually aligns well with CIR task, as it encourages the model to better capture modifications (in T_c). Moreover, we believe including (T_r, T_r) pairs in the contrastive learning helps the learnable text encoder ψ_T^{tr} remain closely aligned with the pre-trained encoder ψ_T .

Refined concatenation of reference and conditioning texts.

As we use "a photo of [\$] that [T_c]" for inference, a naive concatenation strategy also can suffer from training-inference task discrepancy. To tackle this issue, instead of simply concatenating the T_r and T_c , we use the prompt "a photo of [\$] that [T_c]" for updating the text encoder, where [\$] is obtained by the reference caption T_r with the projection module ϕ . Instead of obtaining a pseudo-word token with latent image embedding v , we utilize a textual latent embedding from the reference caption T_r , i.e., $\phi(t_r)$. However, Gu et al. [17] showed that naively replacing the image encoder with the text encoder for the input of ϕ will suffer from the modality gap [25], a phenomenon where text and image embeddings have a gap between them. We tackle this issue by injecting random noise into the textual token representation before it is processed by ϕ , following Gu et al. [17]. More analyses

on variations of noise are in App. B.7.

Fig. 2 illustrates the overview of RTD. We use CLIP backbone and pre-trained projection module ϕ produced by the existing projection-based CIR methods. The text encoder is trained using the proposed loss function (Eq. (1)) while applying the refined batch sampling and concatenation scheme. During inference, the procedure mirrors that of existing projection-based CIR methods, except we utilize the updated text encoder ψ_T^{tr} instead of the frozen one ψ_T . Note that our method only updates the text encoder while the image encoder and the projection module are frozen.

Remark 1: Low data acquisition cost. The text triplets we use can be obtained at a significantly lower cost than CIR triplets. First, the text triplet generation process requires only an easily obtainable caption dataset for generation, whereas other approaches that generate CIR triplets [22, 45, 48] necessitate image or video datasets along with an additional collection phase for semantically similar images or videos. Second, text triplet generation can avoid resource-intensive text-to-image generation [5, 16], making it $15\times$ faster than the CIR triplet generation process used in CompoDiff [16]. Furthermore, if we choose the rule-based text triplet generation strategy, the process becomes $570\times$ faster than the full CIR triplet generation with images; 1M text triplets generation takes just 0.1 hours. Lastly, the storage for the generated text triplets takes up only 100MB, whereas storing a similar quantity of images requires significantly more space (e.g., 400GB for CC3M [39]). More details can be found in App. C.

Table 1. **Training and inference time comparisons.** Purple denotes the additional resource required for RTD. Inference time is measured on a single A100 GPU for a single image. Note that the training hours for SEARLE, LinCIR for 8 A100 GPUs [17] and their RTD variants are trained on 4 A100 GPUs. CompoDiff is trained on 128 A100 and MagicLens is trained on 128 TPUs.

Method	CLIP Backbone	Training (h)	Inference (s)
SEARLE	L/14	4.2h	0.02s
SEARLE (+ RTD)	L/14	4.58h (+0.38h)	0.02s
LinCIR	L/14	0.5h	0.02s
LinCIR (+ RTD)	L/14	0.88h (+0.38h)	0.02s
LinCIR	G/14	0.8h	0.05s
LinCIR (+ RTD)	G/14	3.3h (+2.5h)	0.05s
CompoDiff	L/14	231h	0.12s
MagicLens	L/14	6h	unknown
CIReVL	L/14	-	3.02s

Remark 2: Training and inference efficiency. As reported in Tab. 1, the additional training cost of RTD is small—0.38 hours for ViT-L/14 on 4 A100 GPUs. In contrast, CompoDiff and MagicLens require 231 hours on 128 A100 GPUs and 6 hours on 128 TPUs, respectively, making the cost of RTD negligible. Even with a larger ViT-G/14 backbone, training RTD takes only 2.5 hours on 4 A100 GPUs—still faster than synthetic CIR triplet-based methods and even comparable to SEARLE in ViT-L/14 (4.2h). This training efficiency mainly stems from the advantage of text-only training. As

highlighted by Gu et al. [17], the training complexity for the text encoder is remarkably lower than that for the visual encoder due to the relatively short token lengths of texts (≈ 12) compared to images (256). The average inference time of the CLIP ViT-L/14 image encoder is $\times 3.5$ times slower than that of the text encoder. Another source of efficiency is that RTD requires relatively few iterations (approximately 2000), as the text encoders are already pre-trained and only require minor adjustments to learn the relationships between text triplets. Moreover, in App. B.4, we present a more efficient implementation by selectively updating only a few layers of the text encoder. Along with efficient training, RTD retains the fast inference speed of the original projection-based methods, remaining $150\times$ faster than training-free CIReVL.

4. Experiments

4.1. Experimental setup

Implementation details. We use the AdamW optimizer [29] with a weight decay of 0.01. The learning rate is set to 10^{-5} , with a batch size of 512. We select the text encoder model with the best zero-shot CIRR [28] dev R@1 score for evaluating RTD. We mainly use the visual and textual encoders of the CLIP ViT-L/14 [34] as our backbone. Unless otherwise noted, we use LLM-based 2.5M text triplets provided by CompoDiff [16] for the training. We set the τ as 0.07 in Eq. (1) and scale the standard deviation of Gaussian distribution as 0.5 for the noise injection. More results on various noise distributions can be found in the App. B.7. All experiments were conducted using four NVIDIA A100 GPUs with Python 3.8 and Pytorch [32].

Evaluation datasets and metrics. We compare projection-based CIR methods on five benchmark datasets: CIRR [28], CIRCO [4], FashionIQ [46] (FIQ), COCO object composition [36], and GeneCIS [44]. Details of each dataset are in the App. A.1. For CIRR, FIQ, COCO, and GeneCIS, we have reported their recall scores at the top K retrieval results (R@K). Since the CIRCO dataset includes multiple positive images for each query, we use a ranking-based metric—mean Average Precision scores at the top K results (mAP@K) [10, 30]. For the main results, we compare the results on the FIQ validation split, as well as the test sets of CIRR and CIRCO. For the ablation studies and analyses, the validation splits of these three datasets are utilized. GeneCIS and COCO object composition results and their detailed explanations can be found in the App. B.1.

Baselines. We evaluate the effect of our method when combined with publicly available projection-based ZS-CIR methods: Pic2Word [36], SEARLE [4], LinCIR [17], Context12W [42], and FTI4CIR [26]. All these methods share the similar core concept shown in Fig. 1, but use different training schemes. Pic2Word [36] optimizes contrastive loss between the image embedding and its projected text embed-

Table 2. **Comparison with other baselines.** Note that this comparison is not entirely fair due to differences in backbone models and training data. **Purple** denotes the performance gain from our method, while **red** and **blue** highlight the best and second-best scores, respectively.

Method	Backbone	CIRR			CIRCO			FashionIQ	
		R@1	R@5	R@10	mAP@5	mAP@10	mAP@25	R@10	R@50
Pic2Word [36]	CLIP ViT-L/14	24.2	51.5	64.1	8.3	9.1	10.1	25.3	44.9
+RTD		27.9 (+3.6)	56.2 (+4.8)	68.5 (+4.4)	9.1 (+0.9)	9.6 (+0.5)	10.7 (+0.6)	27.6 (+2.3)	48.9 (+4.0)
SEARLE [4]	CLIP ViT-L/14	24.9	52.3	65.7	11.6	12.7	14.3	25.0	45.3
+RTD		26.6 (+1.7)	56.2 (+3.9)	69.0 (+3.3)	16.5 (+4.9)	17.9 (+5.2)	19.8 (+5.4)	29.3 (+4.4)	50.7 (+5.4)
Context-I2W [42]	CLIP ViT-L/14	25.6	55.4	68.6	-	-	-	27.9	49.1
+RTD		29.2 (+4.6)	58.4 (+3.0)	70.5 (+1.9)	-	-	-	28.1 (+0.2)	49.5 (+0.4)
FTI4CIR [26]	CLIP ViT-L/14	25.9	55.6	67.7	15.1	16.3	18.1	29.4	50.9
+RTD		29.1 (+3.2)	58.8 (+3.2)	70.4 (+2.7)	16.2 (+1.1)	17.4 (+1.1)	19.4 (+1.3)	30.6 (+1.2)	51.7 (+0.8)
LinCIR [17]	CLIP ViT-L/14	23.8	52.9	66.5	13.0	14.1	15.8	27.4	47.7
+RTD		26.6 (+2.9)	56.2 (+3.3)	69.0 (+2.5)	17.1 (+4.1)	18.1 (+4.0)	20.1 (+4.3)	30.2 (+2.8)	51.1 (+3.4)
LinCIR [17]	FSC-CLIP [31] ViT-L/14	33.6	63.1	74.5	14.2	15.4	17.0	28.3	49.5
+RTD		35.9 (+2.3)	67.5 (+4.4)	78.1 (+3.6)	18.3 (+4.1)	19.7 (+4.3)	21.3 (+4.3)	31.2 (+2.9)	52.3 (+2.8)
KEDs [41]	CLIP ViT-L/14	26.4	54.8	67.2	-	-	-	26.8	47.9
CIReVL [20]	CLIP ViT-L/14	24.5	52.3	64.9	18.6	19.0	20.9	28.6	48.6
LDRE [47]	CLIP ViT-L/14	26.5	55.6	67.5	23.4	24.0	26.4	28.5	50.5
MT-CIR [7]	CLIP ViT-L/14	25.5	54.6	67.6	10.4	11.6	13.0	35.4	57.4
MagicLens [48]	CLIP ViT-L/14	30.1	61.7	74.4	29.6	30.8	33.4	30.7	52.5
Compodiff [16]	CLIP ViT-L/14	26.7	55.0	72.6	12.6	13.4	15.8	36.0	48.6
CoVR [45]	BLIP ViT-L/14	39.3	68.2	78.9	-	-	-	27.7	44.6
CASE [22]	BLIP ViT-L/14	35.4	65.8	78.5	-	-	-	-	-
LinCIR [17]	CLIP ViT-G/14	34.9	64.5	76.1	20.6	21.9	24.1	44.5	65.5
+RTD		36.3 (+1.4)	67.5 (+3.0)	78.3 (+2.2)	21.1 (+0.5)	22.3 (+0.4)	24.5 (+0.4)	46.2 (+1.7)	67.3 (+1.8)
Compodiff [20]	CLIP ViT-G/14	34.7	64.3	75.1	15.3	17.7	19.4	39.0	51.7
CIReVL [20]	CLIP ViT-G/14	26.7	55.1	74.5	26.8	27.6	30.0	32.2	52.4
LDRE [47]	CLIP ViT-G/14	36.2	66.4	77.3	31.1	32.2	35.0	32.5	55.4

ding of “a photo of [\$]” to obtain the projection module ϕ . Similarly, SEARLE [4] employs a two-stage approach, starting with an optimization-based textual inversion phase followed by a distillation phase for the projection module ϕ . LinCIR [17] introduces a language-only self-supervised task involving keyword token replacement by letting the original text embedding and the replaced text embedding whose keyword tokens are changed to the projected original text embedding by ϕ . Context-I2W [42] refine the projection module by selecting relevant visual information [42]. Lastly, FTI4CIR [26] separately maps images into subject- and attribute-oriented pseudo-word tokens [26]. Details on how RTD is combined with them can be found in App. A.3.

We train these methods with the CLIP ViT-L/14 in our main experiments. To further verify the compatibility of RTD, we also report results for the ViT-B/32 backbone with SEARLE, Pic2Word, and LinCIR. Moreover, we conduct experiments with a larger backbone (ViT-G/14) and a fine-tuned CLIP model for enhanced compositionality (FSC-CLIP [31]) for LinCIR, enabled by its fast training capability. We use the publicly available pre-trained model for SEARLE (ViT-B/32, ViT-L/14), Pic2Word (ViT-L/14), Context-I2W (ViT-L/14), and FTI4CIR (ViT-L/14). Otherwise, we reproduce the results using the official implementation. When reproducing, we adhere to the same settings in the original papers. For example, we select the final last epoch model for the Pic2Word ViT-B/32 model and choose the model based on the best zero-shot CIRR dev R@1 score for LinCIR. We additionally compare our method with a diverse set of CIR approaches, including another projection-based

ZS-CIR method (KEDs [41]), another attempt to address task discrepancy (MT-CIR [7]), approaches leveraging synthetically generated CIR triplets (CoVR [45], CASE [22], MagicLens [48] and Compodiff [16]), and the training-free methods (CIReVL [20], LDRE [47]).

4.2. Main results

Tab. 2 shows the overview of comparison results with state-of-the-art CIR methods. First, we assess the impact of integrating RTD with existing projection-based CIR methods (SEARLE, Pic2Word, LinCIR, Context-I2W, and FTI4CIR) across CIRR, CIRCO, and FashionIQ. RTD consistently boosts performance, yielding an average improvement of over 2.78 points. This trend also holds for the GeneCIS and COCO object composition datasets, as detailed in App. B.1.

Second, we compare the integration of RTD with those leveraging synthetically generated CIR triplets (CoVR, CASE, MagicLens, and Compodiff). We focus on this comparison to ensure fairness, as leveraging text triplets and updating the textual backbone of RTD may not be fully aligned with the standard projection-based CIR setting. We observe that RTD delivers competitive or superior performance compared to these resource-intensive synthetic CIR triplet-based methods, while being significantly more efficient—over 10–100× faster, as noted in Remark-2 of Sec. 3. For example, with the same CLIP ViT-L/14 backbone, LinCIR + RTD outperforms MagicLens and CoVR in FashionIQ R@10 and R@50 while FTI4CIR + RTD or Context-I2W + RTD achieve performance on par with or exceeding that of MagicLens, MT-CIR, and Compodiff in CIRR metrics.

When combined with larger (ViT-G/14) or fine-tuned (FSC-CLIP) backbones, RTD achieves the best or second-best result on the CIRR and FashionIQ benchmarks. We believe this flexibility of using different backbones underscores the advantage of efficient text-only training of RTD, inherited by LinCIR [17]. We reemphasize that even with a larger backbone like ViT-G/14, RTD remains significantly faster in training than existing synthetic triplet-based methods, as highlighted in Tab. 1.

Lastly, across both backbones (ViT-L/14, G/14), LinCIR + RTD mostly outperforms training-free CReVL and LDRE, except on CIRCO metrics. As shown in Tab. 1, CReVL is significantly slower ($150\times$) than projection-based methods (including RTD), while LDRE incurs even greater inference time due to its ensemble-based strategy.

Table 3. **Ablation study.** Unlike in Tab. 2, for ablation studies and analyses, validation splits of three CIR datasets are used for evaluation. We measure the impact of TCL loss (Eq. (1)), refined batch sampling (RB), and refined concatenation scheme (RC). All models are based on LinCIR ViT-L/14. The first row denotes the vanilla LinCIR without RTD. “Avg” denotes the average of all reported metrics. **Bold** indicates the best result.

TCL				CIRR (R)		CIRCO (mAP)		FIQ (R)		Avg
Text	Anc	RB	RC	@5	@10	@10	@25	@10	@50	
-	-	\times	\times	54.3	67.8	12.7	14.5	27.4	47.7	37.4
(T_r, T_r)	\checkmark	\times	\times	56.0	69.7	13.4	15.2	28.2	48.8	38.5
(T_{r+c}, T_t)	\checkmark	\times	\times	58.2	71.5	14.4	16.0	26.9	47.9	39.2
(T_{r+c}, T_t)	\checkmark	\checkmark	\times	58.2	71.3	15.0	16.7	27.4	49.3	39.6
(T_{r+c}, T_t)	\times	\checkmark	\times	54.3	67.0	12.2	13.6	25.0	45.3	36.3
(T_{r+c}, T_t)	\checkmark	\checkmark	\checkmark	57.9	71.1	16.1	17.8	30.2	51.1	40.7

4.3. Ablation studies

Tab. 3 presents the effectiveness of the proposed components: target-anchored text contrastive loss (TCL), refined batch sampling (RB), and refined concatenation scheme (RC). All evaluation results are on the validation splits. All model variants use ViT-L/14 and a projection module ϕ from LinCIR, making the results in row 1 indicative of the original performance of LinCIR. We first compare the impact of the text pairs fed into TCL loss. We compare our design choice (T_{r+c}, T_t) (from the generated text triplets) with (T_r, T_r) , which is the sole option for constructing a pair given a single conventional caption T_r . The results demonstrate that, on average, using generated triplets (3rd row) is more effective than using original conventional text pairs (2nd row), particularly in the CIRR and CIRCO datasets. In addition, RB (4th row) and RC (6th row) significantly enhance the overall performance, demonstrating the effectiveness of these components. Finally, we measure the impact of using the frozen text encoder for target caption T_t , denoted as “Anchor” in the table. Significant performance degradation is observed when the learnable text encoder is used for extracting the embedding of the target caption T_t (5th row) compared to the target-anchored case (4th row), supporting the importance of the anchoring design choice.

Table 4. T2I retrieval performance of different text encoders on CIRCO val set. “Update (pair)” refers to the setting in the second row of Tab. 3, which uses contrastive learning with the pair (T_r, T_r) . **Bold** indicates the best result, excluding the first row (oracle case).

Query	Text encoder	mAP@5	mAP@10	mAP@25
T_t	Frozen	18.96	19.31	21.05
T_{r+c}	Frozen	10.12	10.71	12.34
T_{r+c}	Update (pair)	10.52	11.15	12.72
T_{r+c}	RTD	15.12	15.80	17.77

4.4. Analyses on our core motivation

We conduct experiments to validate our core motivation (reducing task discrepancy) and verify that the observed gains stem from it. Other details follow Sec. 4.3.

Can RTD really reduce the task discrepancy of the text encoder? We first quantitatively verify whether RTD *indeed* reduces the task discrepancy. We first conduct a controlled experiment that measures the text-to-image (T2I) retrieval performance of the text encoder with conditional texts. We retrieve the target images I_t with the concatenated text query T_{r+c} or the ideal target caption T_t . If our text encoder successfully handles the discrepancy due to the concatenated caption, the text encoder updated by RTD will perform better than the frozen one or “Update (pair)”, which is updated by contrastive learning with the (T_r, T_r) pair (corresponding to row 2 of Tab. 3). We use the CLIP ViT-L/14 and CIRCO [4] validation dataset for evaluation. Since the CIRCO dataset only has CIR triplets (I_r, T_c, I_t) , we use the BLIP [23] captioner to generate T_r and T_t corresponding to the I_r and I_t , respectively. Here, the simple concatenation scheme is applied for the text query T_{r+c} in all cases for a fair comparison. Tab. 4 shows that when the text encoder is either frozen or updated with (T_r, T_r) , the retrieval results using the concatenated caption T_{r+c} are significantly worse than those using the target caption T_t . It supports the claim that the frozen text encoder suffers from the negative effects of task discrepancy between the pretext and CIR tasks. Moreover, it suggests that simply updating the text encoder with (T_r, T_r) pair fails to reduce this discrepancy. In contrast, the text encoder updated by RTD shows a significant improvement over the frozen text encoder or one updated with (T_r, T_r) , showing that it successfully reduces the task discrepancy.

We additionally measure the average cosine similarity between the composed textual features with the prompt “a photo of $\phi(\psi_V(I_r))$ that T_c ” (Fig. 1a) and the target image features (Fig. 1c). The similarity is measured by the LinCIR ViT-L/14 model on the CIRCO validation split. When we use the frozen CLIP text encoder (ψ_T), the average similarity is 0.1. By changing the text encoder to our updated text encoder (ψ_T^{tr}), the similarity becomes 0.29 (+0.19). This result shows again that RTD successfully aligns the composed query features using ϕ to the frozen CLIP image features.

Is all the gain of RTD from naive text-encoder updating? To verify that our improvements cannot be achieved solely

by updating the text encoder backbone without considering the task discrepancy, we additionally measure the results of previous methods (Pic2Word and LinCIR) when naively updating the text encoders. Namely, after training ϕ while keeping all other networks frozen as in previous methods, we additionally update the text encoder using the original loss function, while fixing other modules including ϕ . We denote this update rule as “naïve” in the Tab. 5. Unlike RTD, we observe that just naively updating the text encoder (“naïve”) significantly degrades the performance of the baseline. The results indicate that merely updating the text backbone is not beneficial for CIR; instead, mitigating task discrepancy through RTD is necessary.

Table 5. **Impact of the update scheme.** Two update schemes are compared: (1) using the original objective from baseline (“naïve”) and (2) using RTD. For a fair comparison, in both schemes, ϕ is updated first and ψ_T is updated top on the frozen modules. Other details are the same as Tab. 3.

	CIRR (R)		CIRCO (mAP)		FIQ (R)		Avg
	@5	@10	@10	@25	@10	@50	
Pic2Word	51.4	64.4	8.8	10.1	25.3	44.9	32.2
+naïve	19.2	27.5	1.3	1.6	4.4	11.2	10.9
+ RTD	56.6	69.8	8.8	9.8	27.6	48.9	36.9
LinCIR	54.3	67.8	12.7	14.5	27.4	47.7	36.9
+naïve	52.7	66.8	11.4	13.0	26.3	45.9	35.5
+ RTD	57.9	71.1	16.1	17.8	30.2	51.1	40.7

Next, instead of using the original objective from baselines, we update the text encoder with conventional contrastive learning using the pair (T_r, T_r) , which corresponds exactly to row 2 in Tab. 3 and row 3 in Tab. 4. This setup can also serve as a proxy for the standalone impact of breaking the alignment of pre-trained knowledge, as noted in [3]. As demonstrated in Sec. 4.3, the large gap (more than 2 points) between EPC (last row in Tab. 3) and this proxy (row 2 in Tab. 3) again shows that our gain cannot be attributed to this simple alternative (naive text encoder tuning).

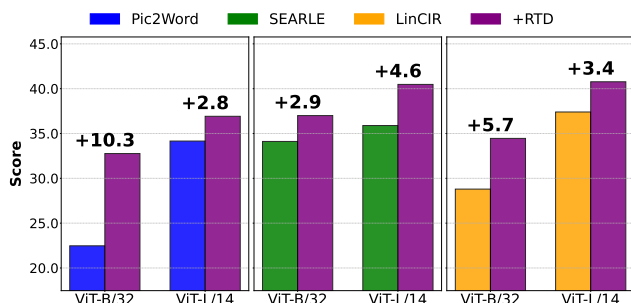


Figure 3. **Impact of sizes of backbone.** The results of RTD combined with Pic2Word [36], SEARLE [4], and LinCIR [17] across different CLIP backbones (ViT-B/32 and ViT-L/14) are shown. Here, the score is the same metric in “Avg” in Tab. 3 and other details are the same as Tab. 3. Full results are in the App. B.2.

4.5. Compatibility across backbone sizes

In the Fig. 3, we observe that the integration of our approach with projection-based CIR methods significantly improves the performance across pioneering projection-based ZS-CIR methods (SEARLE, Pic2Word, and LinCIR) and all backbones (ViT-B/32 and ViT-L/14). For example, regardless of the choice of projection module ϕ and backbones, the minimum performance gain for average scores is greater than 2.8 points. The performance of RTD using the larger backbone (ViT-G/14) can be found in Tab. 2. Details and the full results are provided in the App. B.3. We also provide additional qualitative retrieval results in the App. D.

Table 6. **The effectiveness of different types of text triplets for RTD.** “In-context” denotes an efficient implementation using in-context learning with LLaMA3-8B, without fine-tuning. Details and examples of each text triplet dataset are summarized in Tab. 7 and Tab. 8, respectively. Other details are the same as Tab. 3.

	Source	LLM	CIRR (R)		CIRCO (mAP)		FIQ (R)		Avg
			@5	@10	@10	@25	@10	@50	
LinCIR	-	-	54.3	67.8	12.7	14.5	27.4	47.7	37.4
+RTD	Rule-based	✗	56.7	70.3	15.0	17.0	30.4	51.9	40.2 (+ 2.9)
	IP2P [5]	✓	58.7	71.6	15.9	18.0	29.6	50.7	40.7 (+ 3.3)
	Compodiff [16]	✓	57.9	71.1	16.1	17.8	30.2	51.1	40.7 (+ 3.3)
	In-context	✓	59.3	71.8	15.8	17.5	29.7	51.4	40.9 (+ 3.5)
	CoVR [45]	✓	59.8	72.6	15.4	17.0	29.6	50.8	41.9 (+ 4.5)
	CASE [22]	✓	56.3	69.3	11.1	12.7	26.6	47.8	37.7 (+ 0.3)

4.6. Impact of the text triplet generation strategies

As explained in Sec. 3.1, we evaluate RTD using both 1) publicly available LLM-based text triplets (from IP2P, Compodiff, CoVR, and CASE) along with efficient in-context learning-based text triplets, and 2) LLM-free, rule-based triplets. Tab. 6 shows that RTD consistently improves CIR performance across them (+3.3 for IP2P, +3.3 for Compodiff, +3.5 for in-context learning, +4.5 for CoVR, and +0.31 for CASE, and rule-based triplets achieve 2.9, respectively). We believe this result shows the reproducibility and consistency of RTD, with the rule-based triplets performing comparably to LLM-generated ones, indicating that efficient rule-based triplets are sufficient to achieve strong CIR performance. The marginal improvement in CASE is largely due to the poor quality of text triplets resulting from its construction pipeline that prioritizes CIR triplet quality over text triplet quality, as shown in Tab. 7. Further details can be found in App. A.2, and additional analyses, including data scales related to text triplets, are provided in App. B.5.

5. Conclusion

We presented RTD, a novel post-processing approach that can be easily integrated into existing projection-based CIR methods, aimed at reducing task discrepancy of text encoders. Empirical evaluations demonstrate that RTD significantly boosts the performance of existing projection-based CIR methods across diverse datasets and model backbones, competing with or outperforming other resource-intensive CIR methods with much greater efficiency.

References

- [1] Max Bain, Arsha Nagrani, Gül Varol, and Andrew Zisserman. Frozen in time: A joint video and image encoder for end-to-end retrieval. In *ICCV*, 2021. 2
- [2] Alberto Baldrati, Marco Bertini, Tiberio Uricchio, and Alberto Del Bimbo. Effective conditioned and composed image retrieval combining clip-based features. In *CVPR*, 2022. 1, 3
- [3] Alberto Baldrati, Marco Bertini, Tiberio Uricchio, and Alberto Del Bimbo. Conditioned and composed image retrieval combining and partially fine-tuning clip-based features. In *CVPR*, 2022. 2, 3, 8, 9
- [4] Alberto Baldrati, Lorenzo Agnolucci, Marco Bertini, and Alberto Del Bimbo. Zero-shot composed image retrieval with textual inversion. In *ICCV*, 2023. 1, 2, 3, 5, 6, 7, 8, 9
- [5] Tim Brooks, Aleksander Holynski, and Alexei A Efros. Instructpix2pix: Learning to follow image editing instructions. In *CVPR*, 2023. 1, 3, 5, 8, 2, 9
- [6] Tom Brown, Benjamin Mann, Nick Ryder, Melanie Subbiah, Jared D Kaplan, Prafulla Dhariwal, Arvind Neelakantan, Pranav Shyam, Girish Sastry, Amanda Askell, et al. Language models are few-shot learners. *NeurIPS*, 2020. 1, 3
- [7] Junyang Chen and Hanjiang Lai. Pretrain like you inference: Masked tuning improves zero-shot composed image retrieval. *arXiv preprint arXiv:2311.07622*, 2023. 3, 6
- [8] Ting Chen, Simon Kornblith, Mohammad Norouzi, and Geoffrey Hinton. A simple framework for contrastive learning of visual representations. In *ICML*, 2020. 4
- [9] Yanzhe Chen, Huasong Zhong, Xiangteng He, Yuxin Peng, Jiahuan Zhou, and Lele Cheng. Fashionern: Enhance-and-refine network for composed fashion image retrieval. In *AAAI*, 2024. 3
- [10] Sanghyuk Chun, Wonjae Kim, Song Park, Minsuk Chang, and Seong Joon Oh. Eccv caption: Correcting false negatives by collecting machine-and-human-verified image-caption associations for ms-coco. In *ECCV*, 2022. 5, 1
- [11] Niv Cohen, Rinon Gal, Eli A Meir, Gal Chechik, and Yuval Atzmon. “this is my unicorn, fluffy”: Personalizing frozen vision-language representations. In *ECCV*, 2022. 4
- [12] Ginger Delmas, Rafael S Rezende, Gabriela Csurka, and Diane Larlus. Artemis: Attention-based retrieval with text-explicit matching and implicit similarity. In *ICLR*, 2022. 1, 3
- [13] Yongchao Du, Min Wang, Wengang Zhou, Shuping Hui, and Houqiang Li. Image2sentence based asymmetrical zero-shot composed image retrieval. *ICLR*, 2024. 3
- [14] Abhimanyu Dubey, Abhinav Jauhri, Abhinav Pandey, Abhishek Kadian, Ahmad Al-Dahle, Aiesha Letman, Akhil Mathur, Alan Schelten, Amy Yang, Angela Fan, et al. The llama 3 herd of models. *arXiv preprint arXiv:2407.21783*, 2024. 3, 2
- [15] Yash Goyal, Tejas Khot, Douglas Summers-Stay, Dhruv Batra, and Devi Parikh. Making the v in vqa matter: Elevating the role of image understanding in visual question answering. In *Proceedings of the IEEE conference on computer vision and pattern recognition*, pages 6904–6913, 2017. 1, 2
- [16] Geonmo Gu, Sanghyuk Chun, HeeJae Jun, Yooheon Kang, Wonjae Kim, and Sangdoon Yun. Compodiff: Versatile composed image retrieval with latent diffusion. *arXiv preprint arXiv:2303.11916*, 2023. 1, 2, 3, 5, 6, 8, 9
- [17] Geonmo Gu, Sanghyuk Chun, Wonjae Kim, Yooheon Kang, and Sangdoon Yun. Language-only efficient training of zero-shot composed image retrieval. In *CVPR*, 2024. 1, 2, 3, 4, 5, 6, 7, 8, 9
- [18] Gabriel Ilharco, Mitchell Wortsman, Ross Wightman, Cade Gordon, Nicholas Carlini, Rohan Taori, Achal Dave, Vaishal Shankar, Hongseok Namkoong, John Miller, Hannaneh Hajishirzi, Ali Farhadi, and Ludwig Schmidt. Openclip, 2021. If you use this software, please cite it as below. 5, 7
- [19] Young Kyun Jang, Dat Huynh, Ashish Shah, Wen-Kai Chen, and Ser-Nam Lim. Spherical linear interpolation and text-anchoring for zero-shot composed image retrieval. In *ECCV*, 2024. 3
- [20] Shyamgopal Karthik, Karsten Roth, Massimiliano Mancini, and Zeynep Akata. Vision-by-language for training-free compositional image retrieval. *arXiv preprint arXiv:2310.09291*, 2023. 3, 6, 9
- [21] Seungmin Lee, Dongwan Kim, and Bohyung Han. Cosmo: Content-style modulation for image retrieval with text feedback. In *CVPR*, 2021. 1, 3
- [22] Matan Levy, Rami Ben-Ari, Nir Darshan, and Dani Lischinski. Data roaming and quality assessment for composed image retrieval. In *AAAI*, 2024. 1, 2, 3, 5, 6, 8, 9
- [23] Junnan Li, Dongxu Li, Caiming Xiong, and Steven Hoi. Blip: Bootstrapping language-image pre-training for unified vision-language understanding and generation. In *ICML*, 2022. 7
- [24] Junnan Li, Dongxu Li, Silvio Savarese, and Steven Hoi. Blip-2: Bootstrapping language-image pre-training with frozen image encoders and large language models. In *ICML*, 2023. 3
- [25] Victor Weixin Liang, Yuhui Zhang, Yongchan Kwon, Serena Yeung, and James Y Zou. Mind the gap: Understanding the modality gap in multi-modal contrastive representation learning. *NeurIPS*, 2022. 4
- [26] Haoqiang Lin, Haokun Wen, Xueming Song, Meng Liu, Yupeng Hu, and Liqiang Nie. Fine-grained textual inversion network for zero-shot composed image retrieval. In *SIGIR*, 2024. 1, 2, 3, 5, 6
- [27] Tsung-Yi Lin, Michael Maire, Serge Belongie, James Hays, Pietro Perona, Deva Ramanan, Piotr Dollár, and C Lawrence Zitnick. Microsoft coco: Common objects in context. In *ECCV*, 2014. 1
- [28] Zheyuan Liu, Cristian Rodriguez-Opazo, Damien Teney, and Stephen Gould. Image retrieval on real-life images with pre-trained vision-and-language models. In *ICCV*, 2021. 2, 5, 1
- [29] Ilya Loshchilov and Frank Hutter. Decoupled weight decay regularization. In *ICLR*, 2019. 5
- [30] Kevin Musgrave, Serge Belongie, and Ser-Nam Lim. A metric learning reality check. In *ECCV*, 2020. 5, 1
- [31] Youngtaek Oh, Jae Won Cho, Dong-Jin Kim, In So Kweon, and Junmo Kim. Preserving multi-modal capabilities of pre-trained vlms for improving vision-linguistic compositionality. *EMNLP*, 2024. 2, 6

- [32] Adam Paszke, Sam Gross, Francisco Massa, Adam Lerer, James Bradbury, Gregory Chanan, Trevor Killeen, Zeming Lin, Natalia Gimelshein, Luca Antiga, et al. Pytorch: An imperative style, high-performance deep learning library. *NeurIPS*, 2019. 5
- [33] Khoi Pham, Kushal Kafle, Zhe Lin, Zhihong Ding, Scott Cohen, Quan Tran, and Abhinav Shrivastava. Learning to predict visual attributes in the wild. In *CVPR*, 2021. 1
- [34] Alec Radford, Jong Wook Kim, Chris Hallacy, Aditya Ramesh, Gabriel Goh, Sandhini Agarwal, Girish Sastry, Amanda Askell, Pamela Mishkin, Jack Clark, et al. Learning transferable visual models from natural language supervision. In *ICML*, 2021. 1, 2, 5
- [35] Nils Reimers and Iryna Gurevych. Sentence-bert: Sentence embeddings using siamese bert-networks. *arXiv preprint arXiv:1908.10084*, 2019. 2
- [36] Kuniaki Saito, Kihyuk Sohn, Xiang Zhang, Chun-Liang Li, Chen-Yu Lee, Kate Saenko, and Tomas Pfister. Pic2word: Mapping pictures to words for zero-shot composed image retrieval. In *CVPR*, 2023. 1, 2, 3, 5, 6, 8, 7, 9
- [37] Christoph Schuhmann, Romain Beaumont, Richard Vencu, Cade Gordon, Ross Wightman, Mehdi Cherti, Theo Coombes, Aarush Katta, Clayton Mullis, Mitchell Wortsman, et al. Laion-5b: An open large-scale dataset for training next generation image-text models. *Advances in Neural Information Processing Systems*, 35:25278–25294, 2022. 1
- [38] Christoph Schuhmann, Romain Beaumont, Richard Vencu, Cade Gordon, Ross Wightman, Mehdi Cherti, Theo Coombes, Aarush Katta, Clayton Mullis, Mitchell Wortsman, et al. Laion-5b: An open large-scale dataset for training next generation image-text models. *NeurIPS Dataset and Benchmark*, 2022. 1
- [39] Piyush Sharma, Nan Ding, Sebastian Goodman, and Radu Soricut. Conceptual captions: A cleaned, hypernymed, image alt-text dataset for automatic image captioning. In *ACL*, 2018. 5, 2, 3
- [40] Alane Suhr, Stephanie Zhou, Ally Zhang, Iris Zhang, Hua-jun Bai, and Yoav Artzi. A corpus for reasoning about natural language grounded in photographs. *arXiv preprint arXiv:1811.00491*, 2018. 1
- [41] Yucheng Suo, Fan Ma, Linchao Zhu, and Yi Yang. Knowledge-enhanced dual-stream zero-shot composed image retrieval. *arXiv preprint arXiv:2403.16005*, 2024. 1, 3, 6
- [42] Yuanmin Tang, Jing Yu, Keke Gai, Jiamin Zhuang, Gang Xiong, Yue Hu, and Qi Wu. Context-i2w: Mapping images to context-dependent words for accurate zero-shot composed image retrieval. In *AAAI*, 2024. 1, 2, 3, 5, 6
- [43] Hugo Touvron, Thibaut Lavril, Gautier Izacard, Xavier Martinet, Marie-Anne Lachaux, Timothée Lacroix, Baptiste Rozière, Naman Goyal, Eric Hambro, Faisal Azhar, et al. Llama: Open and efficient foundation language models. *arXiv preprint arXiv:2302.13971*, 2023. 1, 2
- [44] Sagar Vaze, Nicolas Carion, and Ishan Misra. Genecis: A benchmark for general conditional image similarity. In *CVPR*, 2023. 2, 5, 1
- [45] Lucas Ventura, Antoine Yang, Cordelia Schmid, and Gül Varol. CoVR: Learning composed video retrieval from web video captions. 2024. 1, 2, 3, 5, 6, 8, 9
- [46] Hui Wu, Yupeng Gao, Xiaoxiao Guo, Ziad Al-Halah, Steven Rennie, Kristen Grauman, and Rogerio Feris. Fashion iq: A new dataset towards retrieving images by natural language feedback. In *CVPR*, 2021. 2, 5, 1
- [47] Zhenyu Yang, Dizhan Xue, Shengsheng Qian, Weiming Dong, and Changsheng Xu. Ldre: Llm-based divergent reasoning and ensemble for zero-shot composed image retrieval. In *SIGIR*, 2024. 3, 6
- [48] Kai Zhang, Yi Luan, Hexiang Hu, Kenton Lee, Siyuan Qiao, Wenhu Chen, Yu Su, and Ming-Wei Chang. Magiclens: Self-supervised image retrieval with open-ended instructions. *arXiv preprint arXiv:2403.19651*, 2024. 1, 2, 3, 5, 6

An Efficient Post-hoc Framework for Reducing Task Discrepancy of Text Encoders for Composed Image Retrieval

Supplementary Material

A. Additional Implementation Details

A.1. CIR Datasets

FashionIQ [46] is a dataset that contains fashion-related images from three main categories: Shirts, Dresses, and Toptee. It has a total of 30,134 triplets, which were created from 77,684 images. As the ground truth labels are not publicly available, we utilize the results from the validation set for our analysis and comparison. CIRR [28] encompasses a wider range of domains and contains images with more complex descriptions compared to FashionIQ. It contains 36,554 triplets extracted from 21,552 images, which are sourced from the well-known NLVR2 natural language inference dataset [40]. As pointed out in previous works [4, 17, 36], CIRR and FashionIQ suffer from a significant number of false negatives, which can potentially lead to inaccurate retrieval evaluations [4, 36]. To address this issue, CIRCO [4], based on COCO images [27], is recently introduced by providing multiple positive images for each query. This approach enables a more reliable and robust mAP metric [10, 30], which is essential for accurate evaluation of retrieval performance.

We additionally provide results on two more benchmark datasets, GeneCIS [44] and COCO Object Composition introduced by [36], in App. B.1. GeneCIS [44] is also constructed based on COCO images and the Visual Attributes in the Wild dataset [33]. GeneCIS introduces four task variations: (1) focus on an attribute, (2) change an attribute (3) focus on an object, and (4) change an object. These tasks explore different aspects of image retrieval and manipulation. For the COCO Object Composition task, we utilize 5000 images from the COCO validation dataset to evaluate object composition. Our objective is to retrieve an image that contains an object specified by a query image, along with scenes or objects described using text. The composed query is constructed by combining “a photo of [\$], [obj₁], [obj₂] ... and [obj_n]” where [obj_i] are text descriptions.

A.2. Details of text triplets

Here, we describe the details of the LLM-based and rule-based text triplet generation process. As shown in Figs. 4 and 5, which showcases examples of both LLM-based and rule-based triplets, both approaches produce natural and coherent text triplets. Note that none of the datasets used for generating text triplets overlap with the data used in the target CIR benchmarks, with the exception of the CASE dataset [22]. The source of the CASE dataset is VQA2.0 [15], which is constructed from the COCO dataset [27], potentially leading to overlap in cases involving COCO object composition [36].

[Detailed explanation on LLM-based triplets] As described in Sec. 3, besides Compodiff [16], we conduct experiments using various publicly available text triplets: IP2P [5], COVR [45], and CASE [22]. Although the primary objective of these approaches is to generate CIR triplets (I_r, T_c, I_t), they also produce text triplets. Below, we provide detailed descriptions of how text triplets are constructed in each approach (Note again that their final product is CIR triplets). There are two main ways to generate text triplets using LLMs: 1) generating both conditional text T_c and target caption T_t given reference caption T_r using fine-tuned LLM for this task, such as IP2P, Compodiff; and 2) generating only conditional text T_t given pairs (T_r, T_t) from pre-existing captions by identifying with visually or text semantically similar such as CoVR [45], and CASE [22]. In addition to these existing datasets, we implement an efficient in-context learning-based generation process. Examples and summaries of each dataset can be found in Tab. 7 and Tab. 8.

IP2P employs GPT-3 for text triplets generation and fine-tunes it with a human-curated small set of 700 text triplets. Namely, given reference captions T_r sampled from LAION-Aesthetics V2 6.5+ dataset [37], the corresponding conditional texts T_c and corresponding target captions T_t are manually written by humans. After fine-tuning on this small set of text triplets, the model generates 454k text triplets: reference captions T_r from the LAION-Aesthetics V2 6.5+ dataset [37] are provided as input to the fine-tuned LLM, whose output predicts the corresponding conditioning text T_c and the target caption T_t . Note that the LAION-Aesthetics dataset is not related to the original source datasets (FashionIQ, NLVR2, and MS-COCO) used in existing CIR benchmarks (FashionIQ, CIRR, and CIRCO), ensuring no overlap with the CIR benchmarks.

Compodiff enhances the scalability of the IP2P text triplet generation process by modifying the choice of LLM and expanding the fine-tuning dataset. As described in [[16], Section 4], the OPT-6.7B model is utilized and fine-tuned with LoRA on the above 454k text triplets of IP2P [5]. Then, similar to the IP2P approach, given reference captions from the LAION dataset [38], fine-tuned LLM generates the corresponding conditioning texts and target captions.

COVR starts by identifying similar caption pairs from the WebVid2M dataset [1], which contains 2.5 million video-caption pairs. These pairs serve as the reference captions (T_r) and target captions (T_t). Then, given these pairs (T_r, T_t), LLM generates conditional captions that describe the differences between the paired captions. The LLaMA-7B model [43] is utilized for this purpose and is fine-tuned on an expanded version of the above 700 manually annotated triplets used in IP2P (adding 15 annotations for more diverse cases).

CASE uses VQA2.0 dataset [15], which consists of (image, question, answer) triplets. Given (I, Q, A) triplets, complementary triplets (I_c, Q, A_c) are manually selected based on visually similar image I_c with three rules: 1) the premise assumed in question Q holds for both I and I_c , 2) Q is logical for I_c , and 3) the answer A_c for I_c differs from A . Then, conditional text T_c is generated by GPT-3, describing differences between image pairs (I, I_c) without fine-tuning, leveraging in-context learning with a few examples. Since the VQA2.0 dataset is derived from the COCO dataset, COCO captions that match VQA2.0 images are used to form text triplets.

As seen in Tab. 7, compared to other approaches, the quality of the relationships between T_r, T_c , and T_t is not always satisfactory, which results in minimal performance gain as shown in Tab. 6. Namely, unlike other CIR datasets that first create high-quality text triplets before generating CIR triplets, CASE generates the conditioning text T_c using the reference image I_r and target image I_t . The provided reference text T_r and target text T_t are taken directly from the captions of reference image I_r and target image I_t in the VQA2.0 dataset. Therefore, due to the poor descriptiveness of these captions and their lack of consideration for the conditioning text T_c , while T_c can effectively explain the visual differences between I_r and I_t , it often fails to capture the differences between T_r and T_t adequately.

Efficient in-context learning refers to our efficient implementation which uses a recent and powerful LLM, LLaMA3-8B [14]. This approach performs in-context learning using reference captions T_r from the CC3M dataset [39], guided by a custom-designed prompt with a few examples of textual modifications (*e.g.*, replace, change, remove, ...). Specifically, given a reference caption T_r , the prompt instructs the model to generate a target caption T_t , which is a complete sentence that slightly differs from the corresponding reference caption. Then, the prompt guides the model to generate conditioning text that explains the differences between T_r and T_t , based on the above pre-defined textual modifications. Compared to Compodiff, which takes 3.8 hours to generate 1 million text triplets, this version requires only 1.5 hours. In Tab. 6, we verify that this more efficient version achieves competitive performance compared to the other fine-tuned LLM approaches.

Table 7. Examples of text triplet datasets.

Text triplets	Reference text T_r	Conditioning text T_c	Target text T_t
Rule-based	“another wall at my home”	“bedroom is added in place of wall”	“another bedroom at my home”
IP2P [5]	“watercolor of your pet!”	“make it a huge grizzly bear”	“watercolor of a huge grizzly bear!”
Compodiff [16]	“Chinese landscape watercolor painting”	“make the landscape a cityscape”	“chinese cityscape watercolor painting”
Efficient in-context learning	“young business woman on a bench”	“add a laptop”	“young business woman on a bench with a laptop”
CoVR [45]	“Two little boys are running”	“Have them dance”	“Two little boys are dancing”
CASE [22]	“A scone with an orange slice on a plate”	“This food is not acidic”	“a close up of a muffin on a plate on a table”

Table 8. Summaries of text triplet dataset.

Dataset	Use LLM	Model	Fine-tuning strategy	# of text triplets
Rule-based	✗	✗	✗	1.3M
IP2P [5]	✓	GPT-3	Fine-tuned on 700 human-written text triplets	450K
Compodiff [16]	✓	OPT-6.7B	Fine-tuned on 450k IP2P text triplets	2.5M
Efficient in-context learning	✓	LLaMA3-8B	In-context learning	1M
CoVR [45]	✓	LLaMA-7B	Fine-tuned on 700 human-written text triplets	700K
CASE [22]	✓	GPT-3	In-context learning	350K

[Detailed explanation on rule-based triplets] To construct rule-based triplets, we mainly follow the process described in [[16], Section 4.1]. Firstly, given reference captions, important keywords like nouns are extracted with a part-of-speech (POS) tagger via the Spacy library. Then, the keyword is filtered by frequency filtering with hard thresholding to focus only on frequently occurring keywords. Specifically, we only use keywords that appear more than 100. After applying keyword frequency filtering, the remaining keyword list is used to create caption triplets (T_r, T_c, T_t). To generate text triplets, a keyword from the given T_r is selected, and alternative keywords are extracted based on text similarity scores ranging from 0.5 to 0.7, using the SBERT all-MiniLM-L6-v2 [35]. The target caption T_t is then constructed by substituting the original keyword with

a similar alternative. The conditioning text T_c is generated using randomly selected pre-defined templates, as detailed in Tab. 9. Here, most of the templates are similar to that of Compodiff [16]. We use captions from the CC3M dataset [39] as reference captions T_r . Note that CC3M is not related to the existing CIR benchmarks, which again ensures no overlap with the CIR benchmarks.

Since the quality of the generated triplets with the above procedure may not be optimal, we employ an additional filtering process. Compodiff [16] employs an additional filtering process that uses cosine similarities between generated images and texts, calculated by CLIP encoders. However, as we do not have images for captions, we filter the inappropriate texts using only textual information inspired by LinCIR [17]. Namely, we calculate the similarity between the CLIP text embedding of T_t and the CLIP text embedding of “a photo of [\\$]” where [\\$] is obtained by T_t projected by ϕ from LinCIR (ViT-L/14). Following LinCIR noise ($\text{Unif}(0, 1) \times \mathcal{N}(0, 1)$) is injected before passing through ϕ . After calculating the above similarity, texts whose similarities are less than the threshold (0.75) are removed. The same process is also applied to the reference caption T_r and the intersection of filtering processes for T_t and T_r is used for the final dataset whose size becomes 1.3M. As described in App. B.6, we verify that this filtering process is effective. However, this does not imply that the effectiveness of rule-based text triplets is solely dependent on the use of a projection module in the filtering process; even without filtering, the enhancement from RTD remains significant.

```
{
  "source_caption": "what do you do with automobile model for $60 k",
  "target_caption": "what do you do with model for $60 k",
  "relative_caption": "without automobile"
},
{
  "source_caption": "a collage of my latest artwork includes oil pastel and acrylic paintings",
  "target_caption": "a collage of my latest artwork includes water pastel and acrylic paintings",
  "relative_caption": "alter oil to match water"
},
{
  "source_caption": "baseball player hits a home run against sports team",
  "target_caption": "baseball customer hits a home run against sports team",
  "relative_caption": "player is removed and customer takes its place"
},
{
  "source_caption": "another wall at my home",
  "target_caption": "another bedroom at my home",
  "relative_caption": "bedroom is added in place of wall"
},
{
  "source_caption": "tennis player faces a tough schedule if she is to advance",
  "target_caption": "tennis player faces a tough routine if she is to advance",
  "relative_caption": "change schedule to routine"
},
}
```

Figure 4. Example of rule-based triplet datasets

```

{
  "source_caption": "Christopher Nolan got advice from Steven Spielberg before making",
  "target_caption": "Steven Spielberg got advice from Walter Mitty before making",
  "relative_caption": "get advice from Walter Mitty"
},
{
  "source_caption": "by Koh Chip Whye - Black & White Buildings & Architecture",
  "target_caption": "by Koh Chip Whye - Colorful Buildings & Architecture",
  "relative_caption": "make the buildings more colorful"
},
{
  "source_caption": "The Most Hyperrealistic Images Of Beautiful Bathing Women With Their Heads Underwater",
  "target_caption": "The Most Hyperrealistic Images Of Beautiful Bathing Women With Their Heads Underwater and Octopus Arms",
  "relative_caption": "make the women have octopus arms"
},
{
  "source_caption": "Mountains above clouds - p312m1472749 by Mikael Svensson",
  "target_caption": "Mountains on Mars - p312m1472749 by Mikael Svensson",
  "relative_caption": "Put the mountains on Mars"
},
{
  "source_caption": "Le bouquiniste Paris -60x60",
  "target_caption": "The New York City book store -60x60",
  "relative_caption": "Instead of Paris, make it New York."
},
}

```

Figure 5. Example of LLM-based triplet datasets

Table 9. The full 50 keyword converting templates

"replace \${source} with \${target}"	"substitute \${target} for \${source}"
"apply \${target}"	"\${source} is removed and \${target} takes its place"
"convert \${source} to \${target}"	"modify \${source} to become \${target}"
"replace \${source} with \${target}"	"customize \${source} to become \${target}"
"update \${source} to \${target}"	"change \${source} to match \${target}"
"substitute \${target} for \${source}"	"\${target} is introduced after \${source} is removed"
"alter \${source} to match \${target}"	"\${target} is added in place of \${source}"
"upgrade \${source} to \${target}"	"\${target} is introduced as the new option after"
"amend \${source} to fit \${target}"	"\${source} is removed and \${target} is added"
"opt for \${target}"	"\${source} is removed and \${target} is introduced"
"\${source} is removed"	"\${target} is added as a replacement for \${source}"
"add \${target}"	"\${target} is the new option available"
"if it is \${target}"	"\${target} is added after \${source} is removed"
"\${target} is the updated option"	"\${target} is introduced after \${source} is retired"
"\${target} is the updated choice"	"tweak \${source} to become \${target}"
"\${source} is replaced with \${target}"	"has no \${source}"
"change \${source} to \${target}"	"alter \${source} to \${target}"
"swap \${source} for \${target}"	"redesign \${source} as \${target}"
"turn \${source} into \${target}"	"adapt \${source} to fit \${target}"
"choose \${target} instead of \${source}"	"\${target} is the new choice"
"\${target} is the new selection"	"exchange \${source} with \${target}"
"transform \${source} into \${target}"	"show no \${source}"
"no \${source}"	"remove \${source}"
"delete \${source}"	"not a \${source}"
"with no \${source}"	"without \${source}"

A.3. Details on integration with FTI4CIR [26] and Context-I2W [42].

FTI4CIR [26] enhances the fine-grained capability of the projection module ϕ by separately handling subjects and attributes using distinct projection modules, ϕ_s and ϕ_a . To achieve this, they leverage BLIP-generated captions that explicitly separate subject and attribute information in the text domain, formatted as “[primary subject(s)] + [detailed description].” Unlike the subject module ϕ_s , which focuses on global subject information, ϕ_a processes localized attribute details. FTI4CIR extracts attribute features by adaptively aggregating patch features via an additional transformer. However, this approach requires an extra forward pass of the transformer with full sequences of visual embeddings for ϕ_a , rather than a single pooled embedding, making it incompatible with our refined concatenation scheme (RC). Therefore, we do not use ϕ_a during the training of RTD (of course, it is used in inference). Instead, we focus on training ϕ_s while incorporating attribute information in the text domain. Specifically, we generate text triplets using BLIP-generated captions to separately capture subject and attribute information, through “Efficient In-Context Learning” (see App. A.2). Then, we provide subject information to ϕ_s while directly using attribute information in text format. For example, given text triplets: T_r : “a room with a chair and a table”, T_c : “replace the chair with a sofa”, T_t : “a room with a sofa and a table”. our refined concatenation scheme (RC) ensures that only textual subject information is input to ϕ_s . This extraction is feasible because BLIP-generated captions (from FTI4CIR) already provide subject and attribute separation.

Context-I2W [42] introduces a context-dependent projection module that selects relevant visual information. To achieve this, Context-I2W employs a more complex projection mechanism that utilizes context captions such as “A [REPLACE] passes the ball with his teammate during a training session”, which removes the first subject term. Then, these context captions and full visual sequence embeddings from the visual encoder are fused in the Context-I2W projection module. Since it requires full sequences of visual embeddings rather than a single pooled embedding, it can be incompatible with our refined concatenation scheme (RC). In such cases, our method can still be applied simply by replacing the text encoder. Namely, instead of training RTD with this projection module, we simply replace the text encoder with the one updated by RTD using the projection module ϕ from Pic2Word [36]. Namely, during inference, we use the projection module from Context-I2W alongside the RTD-updated text encoder (which was trained with the projection module from Pic2Word). The strong performance of this variant suggests that RTD does not need to be trained with each specific projection module, again highlighting its strong generalizability.

B. Additional experimental results

B.1. Results on GeneCIS [44] and COCO object composition

We observe that integrating our approach with projection-based CIR methods results in consistent yet marginal performance improvements on GeneCIS, as shown in Tab. 10. The relatively smaller performance difference compared to other datasets can be attributed to the discrepancy between the format of the conditioning text of GeneCIS and the projection-based CIR methods training methodology. Namely, GeneCIS only uses the fixed four text instructions “change attribute”, “focus attribute”, “change object” and “focus object”, which is different from the usual text instruction we expected (*e.g.*, “change the dog to a cat”).

In the experiment on COCO object composition, we observe a significant performance improvement, similar to the results obtained on other datasets in Tab. 11. This finding reaffirms that our approach, when combined with ZS-CIR methods, consistently achieves strong performance, demonstrating its generalizability.

B.2. Results on different backbones (ViT-B/32, ViT-L/14)

Tab. 12 summarizes the evaluation results on the FashionIQ dataset. In the table, we observe that the incorporation of our approach with projection-based CIR methods significantly improves the performance across all three existing projection-based CIR methods (SEARLE, Pic2Word, and LinCIR) and all backbones (ViT-B/32 and ViT-L/14). For example, regardless of the choice of projection-based CIR methods and backbones, the minimum performance gain for average R@10 and R@50 scores is greater than 2 and 3.5 points, respectively. Tab. 13 shows a similar trend on the CIRR and CIRCO datasets. Notably, in some metrics on the CIRR and CIRCO datasets, the performance improvements achieved through our method (ViT-B/32) even exceed those obtained by employing a larger backbone (ViT-L/14), which demonstrates the effect of our method. Specifically, in the CIRR R@1 score, SEARLE + RTD (26.29) and LinCIR + RTD (24.82) using ViT-B/32 surpasses the original results of SEARLE (24.89) and LinCIR (23.76) using ViT-L/14.

B.3. Results on larger backbone (ViT-G/14)

As reported in Tab. 2, we evaluate the performance of RTD using the significantly larger backbone (OpenCLIP ViT-G/14 [18]). As described in Sec. 4.3, we use the projection module ϕ from LinCIR [17]. Since the pre-trained projection module ϕ for

Table 10. GeneCIS results

		R@1	Average R@2	R@3
ViT-B	Pic2Word	11.13	21.08	31.05
	+RTD	12.03 (+0.90)	21.61 (+0.53)	31.09 (+0.04)
	SEARLE	12.19	22.56	32.03
	+RTD	12.82 (+0.63)	22.97 (+0.41)	32.44 (+0.41)
	LinCIR	12.23	21.29	30.80
	+RTD	12.83 (+0.60)	22.83 (+1.54)	32.22 (+1.42)
ViT-L	Pic2Word	11.18	21.45	30.55
	+RTD	11.92 (+0.74)	22.32 (+0.87)	31.33 (+0.78)
	SEARLE	12.30	22.08	31.29
	+RTD	12.40 (+0.10)	22.82 (+0.74)	32.37 (+1.08)
	LinCIR	12.45	22.66	32.06
	+RTD	13.18 (+0.73)	23.12 (+0.46)	32.77 (+0.71)

Table 11. COCO object composition results

		R@1	COCO R@5	R@10
ViT-B	Pic2Word	6.88	13.6	17.52
	+RTD	7.62 (+0.74)	20.23 (+6.63)	28.69 (+11.17)
	SEARLE	9.52	21.45	29.38
	+RTD	11.01 (+1.49)	24.34 (+2.89)	32.84 (+3.46)
	LinCIR	7.15	18.38	27.3
	+RTD	9.59 (+2.44)	21.66 (+3.28)	30.66 (+3.36)
ViT-L	Pic2Word	10.26	23.67	32.53
	+RTD	10.26 (+0.00)	24.66 (+0.99)	33.56 (+1.03)
	SEARLE	12.07	26.13	35.17
	+RTD	14.38 (+2.31)	29.74 (+3.61)	38.09 (+2.92)
	LinCIR	11.37	24.53	33.85
	+RTD	14.6 (+3.23)	29.84 (+5.31)	38.87 (+5.02)

LinCIR [17] (ViT-G/14) is not publicly available, we reproduce it and integrate RTD with it. We emphasize that similar to our previous results, RTD again achieves remarkable gains across all datasets. Here, we set the learning rate as 10^{-6} .

B.4. More efficient variants

Tab. 16 presents the results of the more efficient implementations of our approach in terms of the number of updated parameters. Specifically, instead of updating the entire set of parameters of the text encoder, we explore updating only a few layers of the network when applying RTD. Our findings indicate that updating only the fully connected layers (denoted as “Whole FCs”) nearly matches the performance of the full model while using less than half the number of learnable parameters (40.72 vs. 40.53 average scores). Additionally, we verify that updating only three fully connected layers, whose parameter size matches the projection module ϕ and constitutes 11.5% of the full model, is also sufficiently effective. We test various three-layer updating strategies: “First 3 FCs”: the first three layers (closest to the input), “middle 3 FCs”: the middle three layers, “Last 3 FCs”: the last three layers, and “Interleave 3 FCs”: an interleaved selection of three layers (first, middle, and last layers). Among these, we verify that the “Interleave 3 FCs” shows the best result, maintaining competitive performance with the full

Table 12. **FashionIQ validation results.** The results of RTD combined with Pic2Word [36], SEARLE [4], and LinCIR [17] across different CLIP backbones (ViT-B/32 and ViT-L/14) are shown.

		Shirt		Dress		Toptee		Average	
		R@10	R@50	R@10	R@50	R@10	R@50	R@10	R@50
ViT-B/32	Pic2Word	13.40	28.46	8.48	20.77	13.31	29.68	11.73	26.30
	+RTD	23.06 (+9.66)	40.48 (+12.02)	20.33 (+11.85)	41.75 (+20.98)	24.12 (+10.81)	46.35 (+16.67)	22.5 (+10.77)	42.86 (+16.56)
	SEARLE	24.78	41.85	17.90	36.99	25.24	46.71	22.64	41.85
	+RTD	26.69 (+1.91)	44.31 (+2.46)	20.72 (+2.82)	43.13 (+6.14)	26.67 (+1.43)	48.75 (+2.04)	24.7 (+2.06)	45.4 (+3.55)
	LinCIR	18.55	34.64	15.67	33.86	20.19	40.08	18.14	36.20
	+RTD	23.65 (+5.10)	42.74 (+8.10)	19.98 (+4.31)	41.75 (+7.89)	24.73 (+4.54)	46.56 (+6.48)	22.79 (+4.65)	43.68 (+7.48)
ViT-L/14	Pic2Word	26.59	42.93	21.32	43.53	28.10	48.19	25.34	44.88
	+RTD	27.97 (+1.38)	46.96 (+4.03)	23.50 (+2.18)	46.65 (+3.12)	31.31 (+3.21)	53.09 (+4.90)	27.59 (+2.25)	48.90 (+4.02)
	SEARLE	26.94	45.34	19.58	40.80	28.45	49.77	24.99	45.30
	+RTD	32.63 (+5.69)	50.39 (+5.05)	23.2 (+3.62)	47.25 (+6.45)	32.18 (+3.73)	54.56 (+4.79)	29.34 (+4.35)	50.73 (+5.43)
	LinCIR	30.42	47.99	21.86	44.77	29.98	50.38	27.42	47.71
	+RTD	32.83 (+2.41)	50.44 (+2.45)	24.49 (+2.63)	48.24 (+3.47)	33.4 (+3.42)	54.56 (+4.18)	30.24 (+2.82)	51.08 (+3.37)

Table 13. **CIRR and CIRCO test results.** Details are the same as Tab. 12.

		R@1	CIRR		R@10	mAP@5	CIRCO		
			R@5	R@5			mAP@10	mAP@25	mAP@50
ViT-B/32	Pic2Word	13.64	37.45	52.22	2.85	3.24	3.89	4.31	
	+RTD	23.59 (+9.95)	51.76 (+14.31)	65.16 (+12.94)	6.39 (+3.54)	6.66 (+3.42)	7.64 (+3.75)	8.16 (+3.85)	
	SEARLE	23.71	53.3	66.84	8.90	9.42	10.64	11.34	
	+RTD	26.29 (+2.58)	56.41 (+3.11)	69.74 (+2.90)	11.26 (+2.36)	12.11 (+2.69)	13.63 (+2.99)	14.37 (+3.03)	
	LinCIR	18.87	45.66	58.43	6.25	6.74	7.62	8.10	
	+RTD	24.82 (+5.95)	53.47 (+7.81)	66.87 (+8.44)	8.94 (+2.69)	9.35 (+2.61)	10.57 (+2.95)	11.21 (+3.11)	
ViT-L/14	Pic2Word	24.22	51.49	64.05	8.27	9.10	10.09	10.75	
	+RTD	27.86 (+3.64)	56.24 (+4.75)	68.48 (+4.43)	9.13 (+0.86)	9.63 (+0.53)	10.68 (+0.59)	11.27 (+0.52)	
	SEARLE	24.89	52.31	65.69	11.62	12.72	14.33	15.13	
	+RTD	26.63 (+1.74)	56.17 (+3.86)	68.96 (+3.27)	16.53 (+4.91)	17.89 (+5.17)	19.77 (+5.44)	20.68 (+5.55)	
	LinCIR	23.76	52.89	66.46	13.00	14.11	15.81	16.68	
	+RTD	26.63 (+2.87)	56.17 (+3.28)	68.96 (+2.50)	17.11 (+4.11)	18.11 (+4.00)	20.06 (+4.25)	21.01 (+4.33)	

Table 14. FashionIQ results on larger OpenCLIP ViT-G/14 backbone [18].

Method	Shirt		Dress		Toptee		Average	
	R@10	R@50	R@10	R@50	R@10	R@50	R@10	R@50
LinCIR (reported in [17])	46.76	65.11	38.08	60.88	50.48	71.09	45.11	65.69
LinCIR (reproduced)	46.61	64.72	38.18	60.54	49.26	70.83	44.68	65.36
+RTD	47.20 (+0.59)	66.24 (+1.52)	39.86 (+1.68)	63.01 (+2.47)	51.56 (+2.30)	72.51 (+1.68)	46.21 (+1.54)	67.26 (+1.90)

Table 15. CIRR and CIRCO results on larger OpenCLIP ViT-G/14 backbone [18].

ViT-G	R@1	CIRR		R@10	mAP@5	CIRCO		
		R@5	R@5			mAP@10	mAP@25	mAP@50
LinCIR (reported in [17])	35.25	64.72	76.05	19.81	21.01	23.03	24.18	
LinCIR (reproduced)	34.94	64.51	76.12	20.63	21.93	24.12	25.20	
+RTD	36.31 (+1.37)	67.47 (+2.96)	78.31 (+2.19)	21.08 (+0.45)	22.29 (+0.36)	24.46 (+0.34)	25.44 (+0.24)	

model (40.72 vs. 39.88 average scores). We believe these findings suggest a promising direction for enhancing the training efficiency of our approach by selectively updating only specific layers of the text encoder.

Table 16. **More efficient variants.** “Learnable params (%)” denotes the percentage of learnable parameters relative to the entire set of parameters in the text encoder.

Training variants	Learnable params (%)	CIRR		CIRCO		FashionIQ		Avg
		R@5	R@10	mAP@10	mAP@25	R@10	R@50	
Baseline(LinCIR)	0%	54.29	67.76	12.67	14.45	27.42	47.71	37.38
+RTD (Full model)	100%	57.90	71.13	16.10	17.84	30.24	51.08	40.72
+RTD (Whole FCs)	45.8%	57.76	71.35	15.03	16.90	30.31	51.81	40.53
+RTD (Front 3 FCs)	11.5%	55.65	69.83	13.95	15.81	28.69	49.92	38.98
+RTD (Middle 3 FCs)	11.5%	56.69	70.03	14.66	16.58	28.55	49.84	39.39
+RTD (Last 3 FCs)	11.5%	56.84	69.74	14.81	16.70	29.16	50.43	39.61
+RTD (Interleave 3 FCs)	11.5%	57.21	70.65	15.20	17.13	28.91	50.17	39.88

B.5. Effectiveness of RTD across dataset scales

We conduct experiments with various scales of training text triplets. For the small-scale text triplets, we sub-sampled text triplets from LLM-based text triplets. Thus, the last row in the Tab. 17 denotes the original result (LLM-based RTD result). We also measure the effectiveness of RTD using large-scale text triplets (up to 5M) by combining publicly available text triplets (IP2P, CoVR) with ours (LLM-based, rule-based). Here, validation splits of all three benchmark datasets are utilized and full results will be included in the final version.

As shown in Tabs. 17 and 18, we confirm that small-scale text triplets are sufficient to achieve the effectiveness of RTD. We believe the main reason for this is that, to reduce task discrepancy, only the relationship between the concatenated caption (reference caption + conditioning caption, T_{r+c}) and the target caption T_t needs to be learned. We believe this learning task requires much less data compared to learning representations from scratch. Moreover, since the text encoder is already pre-trained, the model does not need significant changes to learn this simple but crucial learning task for CIR.

Table 17. **Results across different scales of LLM-based text triplets.** In each row, text triplets are sub-sampled from 2.5M original LLM-based text triplets provided by Compodiff [16]

# of triplets	CIRR R@5	CIRCO mAP@10	FashionIQ R@10	Avg
1K	56.64	15.66	29.89	34.06
50K	57.40	15.95	30.77	34.71
100K	57.16	16.03	30.57	34.59
2.5M	57.90	16.10	30.24	34.75

Table 18. Results of larger-sized text triplets

IP2P	CoVR	Compodiff	Template-based	CIRR R@5	CIRCO mAP@10	FashionIQ R@10	Avg	# of triplets
✓				58.65	15.94	29.62	34.74	450k
	✓			59.82	15.35	29.58	34.92	700k
		✓		57.90	16.10	30.24	34.75	2.5M
			✓	56.71	15.01	30.37	34.03	1.3M
✓	✓			59.32	16.10	30.81	35.41	1.25M
✓	✓	✓		59.08	16.15	30.97	35.40	3.75M
✓	✓	✓	✓	58.65	16.54	31.22	35.47	5.05M

B.6. Ablations on filtering process

In rule-based text triplet generation, we highlight that the filtering process using the projection module from LinCIR is *marginally effective*. As demonstrated in the Tab. 19, even without the filtering procedure, the enhancement of RTD from LinCIR remains considerable. This result demonstrates that the effectiveness of our rule-based text triplets is not solely dependent on the use of the projection module from LinCIR in the filtering process.

Table 19. Ablations on filtering process

Type	LinCIR-based filtering	CIRR R@5	CIRCO mAP@10	FashionIQ R@10	Avg
LinCIR	-	54.29	12.67	27.42	31.46
+RTD (rule-based)	✗	55.49	14.75	30.24	33.49
+RTD (rule-based)	✓	56.71	15.01	30.37	34.03

B.7. Ablations on noise injection

We conduct an ablation study of the different noise types employed for the “refined concatenation scheme” shown in Fig. 2. We compare three different noise types, uniform distribution, Gaussian distribution, and LinCIR-ish noise ($\text{Unif}(0, 1) \times \mathcal{N}(0, 1)$). We also examine the scale of LinCIR-ish noise from 0.1, 0.5, and 1. We report the test scores for CIRR and CIRCO, as well as the FashionIQ validation scores for Pic2Word, SEARLE, and LinCIR in Tab. 20 and Tab. 21. In the tables, we observe that all noise distributions show decent performance and LinCIR-like noises show slightly better performances than uniform distribution and normal distribution. We also observe that the different scale choice for the LinCIR-like noise somewhat affects the overall performances. In the main experiments, we chose 0.5 for the noise scale, following the observed performance improvements.

C. Generating text triplets cost

Although generating text triplets is not our main contribution, for comprehensive understanding, we compare the generation time of LLM-based and rule-based approaches. Even when using LLMs, constructing text triplets is significantly more cost-effective than CIR triplets. Specifically, CIR triplets involve: 1) a subsequent, computationally intensive text-to-image generation phase [5, 16], or 2) the availability of image or video datasets along with an additional collection phase for semantically similar images or videos [22, 45]. In contrast, generating text triplets bypasses these resource-heavy steps. For example, using 8 A100 GPUs, generating 1M text triplets takes 0.1 hours with the rule-based approach and 3.8 hours with the LLM-based approach from Compodiff [16] (OPT-6.7B). As described in App. A.2, a more efficient text triplet generation method using in-context learning with LLaMA3-8B reduces the generation time to 1.5 hours without the need for fine-tuning.

Therefore, while generating text triplets with LLMs incurs a higher cost compared to rule-based methods, it is still significantly faster (15 times) than generating CIR triplets (as used in CompoDiff), which utilize the text generation step as a preliminary phase for subsequent text-to-image generation. Thus, we believe LLM-based generation remains viable, but the rule-based approach is more efficient.

D. Qualitative example on CIRCO

We qualitatively illustrate the results of incorporating RTD into LinCIR on the CIRCO dataset in Fig. 6. The visual examples provide an intuitive demonstration of how the integration of RTD enhances the performance of LinCIR, effectively capturing the semantic meaning of the modification descriptions while preserving the relevant visual information from the reference image.

E. Discussion and Limitations

We have primarily focused on evaluating the integrability of RTD with representative projection-based CIR methods [4, 17, 36]. However, we have not yet explored or tested the extensibility of RTD to other CIR approaches that achieve strong performance, such as those utilizing human-annotated CIR triplets (supervised) [3], synthetically generated CIR triplets [16, 22, 45], or training-free methods [20]. Given the core motivation behind RTD, its adaptability to those CIR approaches that directly train fusion modules or backbones using CIR triplets may be limited. However, considering the strong performance and practical advantages—such as efficient training and inference—offered by projection-based CIR methods compared to other variants, we believe that integrating RTD with them remains a valuable direction in the CIR domain.

Table 20. Noise type variation on CIRR/CIRCO dataset

		Noise type	Scale	CIRR			CIRCO			
				R@1	R@5	R@10	mAP@5	mAP@10	mAP@25	mAP@50
ViT-B/32	Pic2Word	-	-	13.64	37.45	52.22	2.85	3.24	3.89	4.31
	+RTD	Unif(-1,1)	1	23.23	50.55	64.28	4.29	4.57	5.19	5.57
		$\mathcal{N}(0, 1)$	1	21.18	47.78	61.47	4.09	4.26	4.83	5.17
		$\mathcal{N}(0, 1) \times \text{Unif}(0,1)$	0.1	23.52	51.13	64.53	5.13	5.46	6.17	6.62
		$\mathcal{N}(0, 1) \times \text{Unif}(0,1)$	0.5	23.01	51.18	64.84	4.29	4.57	5.19	5.57
		$\mathcal{N}(0, 1) \times \text{Unif}(0,1)$	1	23.59	51.76	65.16	6.39	6.66	7.64	8.16
	SEARLE	-	-	23.71	53.3	66.84	8.9	9.42	10.64	11.34
	+RTD	Unif(-1,1)	1	26.07	55.98	69.18	10.87	11.55	12.97	13.65
		$\mathcal{N}(0, 1)$	1	26.41	56.68	69.47	10.91	11.53	12.88	13.6
		$\mathcal{N}(0, 1) \times \text{Unif}(0,1)$	0.1	26.02	55.47	68.15	10.43	11.07	12.37	13.07
$\mathcal{N}(0, 1) \times \text{Unif}(0,1)$		0.5	26.29	56.41	69.74	11.26	12.11	13.63	14.37	
$\mathcal{N}(0, 1) \times \text{Unif}(0,1)$		1	26.43	56.58	69.76	11.42	12.04	13.38	14.1	
LinCIR	-	-	18.87	45.66	58.43	6.25	6.74	7.62	8.1	
+RTD	Unif(-1,1)	1	24.39	52.77	66.39	6.81	7.27	8.28	8.84	
	$\mathcal{N}(0, 1)$	1	24.63	53.52	66.63	7.6	7.97	8.92	9.49	
	$\mathcal{N}(0, 1) \times \text{Unif}(0,1)$	0.1	24.58	53.3	66.65	9.6	10.11	11.47	12.15	
	$\mathcal{N}(0, 1) \times \text{Unif}(0,1)$	0.5	24.82	53.47	66.87	8.94	9.35	10.57	11.21	
	$\mathcal{N}(0, 1) \times \text{Unif}(0,1)$	1	25.4	54.58	67.69	8.17	8.53	9.72	10.35	
ViT-L/14	Pic2Word	-	-	24.22	51.49	64.05	8.27	9.1	10.09	10.75
	+RTD	Unif(-1,1)	1	28.24	55.95	68.77	8.14	8.81	9.83	10.37
		$\mathcal{N}(0, 1)$	1	27.06	53.95	66.43	7.08	7.66	8.57	9.07
		$\mathcal{N}(0, 1) \times \text{Unif}(0,1)$	0.1	28.24	57.35	68.65	10.04	10.63	11.71	12.31
		$\mathcal{N}(0, 1) \times \text{Unif}(0,1)$	0.5	27.86	56.24	68.48	9.13	9.63	10.68	11.27
		$\mathcal{N}(0, 1) \times \text{Unif}(0,1)$	1	27.71	55.68	68.02	8.14	8.78	9.84	10.35
	SEARLE	-	-	24.89	52.31	65.69	11.62	12.72	14.33	15.13
	+RTD	Unif(-1,1)	1	26.96	56.99	69.52	15.82	16.78	18.54	19.39
		$\mathcal{N}(0, 1)$	1	27.66	57.54	69.57	15.24	15.93	17.65	18.44
		$\mathcal{N}(0, 1) \times \text{Unif}(0,1)$	0.1	26.31	55.88	69.4	16.05	17.26	19.12	20.01
$\mathcal{N}(0, 1) \times \text{Unif}(0,1)$		0.5	27.04	56.82	69.95	16.53	17.89	19.77	20.68	
$\mathcal{N}(0, 1) \times \text{Unif}(0,1)$		1	27.93	57.76	70.19	17.35	18.66	20.52	23.44	
LinCIR	-	-	23.76	52.89	66.46	13	14.11	15.81	16.68	
+RTD	Unif(-1,1)	1	26.58	56.31	68.94	17.23	18.2	20.11	21.03	
	$\mathcal{N}(0, 1)$	1	26.75	55.64	68.48	16.45	17.57	19.37	20.3	
	$\mathcal{N}(0, 1) \times \text{Unif}(0,1)$	0.1	26.7	56.22	69.08	17.24	18.27	20.24	21.19	
	$\mathcal{N}(0, 1) \times \text{Unif}(0,1)$	0.5	26.63	56.17	68.96	17.11	18.11	20.06	21.01	
	$\mathcal{N}(0, 1) \times \text{Unif}(0,1)$	1	26.99	56.1	69.01	17.33	18.3	20.21	21.13	

F. Societal Impacts

Although our paper demonstrates promising outcomes in the ZS-CIR task, further examination of the data and the model is essential prior to practical deployment. Since our method focuses mainly on optimization for accuracy, unwanted social implications can occur. For example, real-world images from databases and user-generated text may inadvertently cause harmful cases.

G. Reproducibility Statement

We provide all necessary details for reproduction in the manuscript, including implementation details, metrics, datasets, and baselines, as described in Sec. 4.1. Additionally, the training and evaluation dataset details are elaborated in Apps. A.1 and A.2. The anonymized code for reproducing our results is provided in the supplementary material.

Table 21. Noise type variation on FashionIQ dataset

	Noise type	Scale	Shirt		Dress		Toptee		Average		
			R@10	R@50	R@10	R@50	R@10	R@50	R@10	R@50	
ViT-B/32	Pic2Word	-	-	13.4	28.46	8.48	20.77	13.31	29.68	11.73	26.3
	+RTD	Unif(-1,1)	1	21.84	37.63	18.49	39.61	23.0	43.91	21.11	40.38
		$\mathcal{N}(0, 1)$	1	20.36	37.54	16.16	38.18	21.67	42.48	19.4	39.4
		$\mathcal{N}(0, 1) \times \text{Unif}(0,1)$	0.1	22.23	39.35	19.98	41.7	23.81	45.23	22.01	42.09
		$\mathcal{N}(0, 1) \times \text{Unif}(0,1)$	0.5	24.53	43.82	20.33	41.55	26.01	48.75	23.62	44.7
		$\mathcal{N}(0, 1) \times \text{Unif}(0,1)$	1	23.06	40.48	20.33	41.75	24.12	46.35	22.5	42.86
	SEARLE	-	-	24.78	41.85	17.90	36.99	25.24	46.71	22.64	41.85
	+RTD	Unif(-1,1)	1	23.75	42.25	20.18	40.36	25.14	46.46	23.02	43.02
		$\mathcal{N}(0, 1)$	1	24.14	42.25	20.23	40.16	24.17	46.35	22.85	42.92
		$\mathcal{N}(0, 1) \times \text{Unif}(0,1)$	0.1	25.12	44.85	20.92	41.40	26.57	47.63	24.20	44.62
		$\mathcal{N}(0, 1) \times \text{Unif}(0,1)$	0.5	26.69	44.31	20.72	43.13	26.67	48.75	24.70	45.40
		$\mathcal{N}(0, 1) \times \text{Unif}(0,1)$	1	25.07	44.01	20.43	41.00	26.11	47.12	23.87	44.04
	LinCIR	-	-	18.55	34.64	15.67	33.86	20.19	40.08	18.14	36.20
	+RTD	Unif(-1,1)	1	21.79	39.35	18.89	40.21	23.66	45.33	21.45	41.63
		$\mathcal{N}(0, 1)$	1	22.37	38.67	19.53	40.11	23.71	44.37	21.87	41.05
		$\mathcal{N}(0, 1) \times \text{Unif}(0,1)$	0.1	23.95	44.11	19.83	41.99	26.62	47.58	23.47	44.56
$\mathcal{N}(0, 1) \times \text{Unif}(0,1)$		0.5	23.65	42.74	19.98	41.75	24.73	46.56	22.79	43.68	
$\mathcal{N}(0, 1) \times \text{Unif}(0,1)$		1	22.82	41.12	19.78	41.70	25.09	47.07	22.56	43.29	
ViT-L/14	Pic2Word	-	-	26.59	42.93	21.32	43.53	28.10	48.19	25.34	44.88
	+RTD	Unif(-1,1)	1	27.87	45.93	23.90	46.80	31.21	52.22	27.66	48.32
		$\mathcal{N}(0, 1)$	1	26.94	44.95	23.45	45.56	30.34	51.45	26.91	47.32
		$\mathcal{N}(0, 1) \times \text{Unif}(0,1)$	0.1	28.26	47.64	24.05	47.20	31.21	53.70	27.84	49.51
		$\mathcal{N}(0, 1) \times \text{Unif}(0,1)$	0.5	27.97	46.96	23.50	46.65	31.31	53.09	27.59	48.90
		$\mathcal{N}(0, 1) \times \text{Unif}(0,1)$	1	28.41	46.91	24.10	46.21	31.11	52.27	27.87	48.46
	SEARLE	-	-	26.94	45.34	19.58	40.80	28.45	49.77	24.99	45.30
	+RTD	Unif(-1,1)	1	30.13	46.57	22.16	46.90	28.76	50.74	27.02	48.07
		$\mathcal{N}(0, 1)$	1	26.99	43.23	21.17	44.82	27.54	49.06	25.23	45.70
		$\mathcal{N}(0, 1) \times \text{Unif}(0,1)$	0.1	32.63	50.39	23.20	47.25	32.18	54.56	29.34	50.73
		$\mathcal{N}(0, 1) \times \text{Unif}(0,1)$	0.5	31.80	49.31	23.20	47.30	31.41	54.00	28.80	50.20
		$\mathcal{N}(0, 1) \times \text{Unif}(0,1)$	1	30.03	47.06	22.41	47.05	30.39	52.42	27.61	48.84
	LinCIR	-	-	30.42	47.99	21.86	44.77	29.98	50.38	27.42	47.71
	+RTD	Unif(-1,1)	1	31.94	50.10	24.44	48.19	33.04	54.26	29.81	50.85
		$\mathcal{N}(0, 1)$	1	31.70	49.41	23.90	48.19	33.23	53.54	29.27	50.38
		$\mathcal{N}(0, 1) \times \text{Unif}(0,1)$	0.1	32.92	50.64	24.49	48.74	33.50	55.02	30.31	51.47
$\mathcal{N}(0, 1) \times \text{Unif}(0,1)$		0.5	32.83	50.44	24.49	48.24	33.40	54.56	30.24	51.08	
$\mathcal{N}(0, 1) \times \text{Unif}(0,1)$		1	32.43	50.54	24.64	48.79	33.25	54.77	30.11	51.36	



Figure 6. Qualitative Results on CIRCO dataset